Digital Object Identifier 10.1109/TPWRD.2023.3244853.

IEEE Transactions on Power Delivery

A Fault Detection Algorithm Based on Artificial Neural Network Threshold Selection in Multi-Terminal DC Grids

Alireza Pourfaraj
Hossein Iman-Eini
Sattar Bazyar
Saeid Ahmadi
Ehsan Asadi
Marius Langwasser
Marco Liserre

Suggested Citation

A. Pourfaraj et al., "A Fault Detection Algorithm Based on Artificial Neural Network Threshold Selection in Multi-Terminal DC Grids," in IEEE Transactions on Power Delivery, vol. 38, no. 4, pp. 2510-2520, Aug. 2023,

A Fault Detection Algorithm Based on Artificial Neural Network Threshold Selection in Multi-Terminal DC Grids

Alireza Pourfaraj, Hossein Iman-Eini, *Senior Member, IEEE*, Sattar Bazyar, Saeid Ahmadi , Ehsan Asadi, Marius Langwasser, *Member, IEEE*, Marco Liserre, *Fellow, IEEE*

***Abstract*— The DC fault is one of the critical challenges in the High Voltage Multi-Terminal Direct Current (HV-MTDC) grid. The fixed value threshold used in some implementations may be affected by different grid conditions and thus causes errors in the fault detection procedure. This paper offers a two-stage fault detection algorithm based on the integrated Artificial Neural Network (ANN) and Discrete Wavelet Transform (DWT) theory. The main innovations of the proposed method are: 1) Increasing the reliability of the fault detection operation by solving the fixed value threshold problems; 2) Offering high robustness against the wide range of fault resistances; 3) Providing bus protection capability and 4) Setting relays locally, and avoiding the requirement to high-speed communications links. Also, it offers DC fault detection in a short period of time. The performance of the proposed protection scheme has been ascertained via simulations in the MATLAB/Simulink environment. The results prove the robustness of the proposed method against noise disturbance, high resistance fault, and grid parameters variations.**

***Index Terms*— Adaptive threshold, artificial neural network (ANN), discrete wavelet transform (DWT), high voltage multi-terminal direct current (HV-MTDC), modular multilevel converter (MMC).**

I. Introduction

HIGH Voltage Multi-Terminal Direct Current (HV-MTDC) systems based on the Modular Multilevel Converter (MMC) are broadly used to transmit the power produced by renewable sources owing to their competency to transfer energy in abundant amounts [1]-[2]. Likewise, flexibility, redundancy, less asset, reliability, and more controllability have made employing the HV-MTDC system more attractive [3]-[4]. Although these systems have many proficiencies, they confront some concerns. A critical concern is the rapid spread of DC faults due to low DC grid impedance, a drastic challenge to system reliability [5]. Thus, providing a proper manner for fast DC fault detection is vital in preventing the immediate propagation of fault in the MTDC grid.

Moreover, only the faulty line must be disconnected from the grid in the MTDC system. Hence, grid protection must be selective and highly reliable [6]. In this respect, some articles proposed numerous methods for accurate fault detection. The existing techniques can be classified into unit protection and non-unit protection. The unit protection methods presented in [7] and [8] collect the voltage and current from different grid parts, and the final detection decision is made based on it. The significant detriment of the proposed method is the need for a fast telecommunication link, which is costly and reduces reliability. Authors in [9] presented a non-unit protection method to solve the problems caused by unit protection schemes. This method provides a short delay and high reliability.

The unit protection methods depend on the boundary effect of DC inductors located at both ends of transmission lines. The inherent boundary property of current-limiting inductors is used to design the boundary protection scheme to distinguish between internal and external faults [10]-[11]. However, non-unit protection schemes can be categorized into four groups based on the boundary effect, I) Rate of Change of Voltage (ROCOV), II) Time domain method, III) Frequency-based methods, and IV) Artificial intelligence-based methods.

Reference [12] determines the ROCOV across the current limiting inductor for fault detection while its precision diminishes in high-resistance faults. The Traveling Waves (TWs) approach is introduced in [13]–[15]. This method imposes a high cost due to using high-precision measuring equipment. In addition, it suffers from low robustness against noise and extreme susceptibility to gird transients.

Frequency-based attitudes are presented in some publications to tackle the defects of time-based techniques. In this respect, [16] employed the Short-Term Fourier Transform (STFT) scheme. Although the introduced method has quick fault detection capability, its time-frequency resolution is inappropriate. In [17], the frequency-domain S transform detects the DC fault. Even though the suggested scheme is highly dependable, it is not noise resistant. Authors in [18] also introduced the Discrete Wavelet Transform (DWT) strategy to extract time and the transient signal frequency details. The transient signal energy is computed and compared with the fixed value threshold. These methods have a significant computational burden and are also not robust to system disturbance owning applying a fixed value threshold.

References [19] and [20] accomplished fault detection with high precision and speed via transient energy calculation and selected the appropriate mother wavelet function. However, the significant weakness of these methods is using a large number of fixed value thresholds, reducing the protection system's reliability. In addition, this method depends on the voltage or current derivative, which causes the protection system's malfunction in the presence of noise. Besides, they have not offered a systematic method to differentiate between overhead lines (OHLs) fault and bus fault protection. In addition, all the approaches above used fixed value thresholds, reducing the reliability of the protection system.

The Artificial Neural Network (ANN), which has pattern recognition capability, is one of the most dominant techniques for solving non-linear problems [21], [22]. In [23], the thirteen ANN units are employed for fault detection, increasing the workload and complexity. In [24], although the fault detection delay is small, the impact of noise is not investigated. Authors in [25] used the combination of Fast Fourier Transform (FFT) and ANN, which causes a large fault detection delay. The combination of DWT and a Fuzzy neural network using a high sampling frequency is proposed in [26]. However, the proposed method's performance is not examined in the presence of noise. Authors in [27] employed the integration of DWT and ANN. Although it offers high accuracy in different fault resistances, the fixed value threshold is used for activating the fault detection algorithm. In addition, the impact of grid parameter variation is not studied in the above approaches.

In this article, inspired by the abovementioned challenges, a novel and straightforward fault detection algorithm is presented, combining the ANN and DWT methods. One of the significant features of the proposed method is the appropriate threshold selection by ANN agreeing to different MTDC grid conditions. Hence, the protection system reliability is guaranteed by eliminating the conventional fixed value thresholds. Moreover, using ANN as a trigger of the fault detection algorithm increases the protection system robustness against non-faulty case studies. Besides, the proposed strategy's selectivity is ensured by appropriately recognizing the type of fault (internal or external).

Additionally, using two ANN units, the mentioned conditions are fulfilled, reducing the protection system's complexity in terms of threshold setting of protection relays, ANN structure, and local measurements. Moreover, a bus fault detection unit is employed in the proposed strategy.

The remainder of the article is categorized as follows: Section II describes the MMC-based four-terminal DC grid with its OHLs. Section III introduces the ANN method, wavelet theory, and DC reactor boundary effect. The presented method is scrutinized in section IV, its performance is evaluated in Section V, then a comparison is made in section VI. Finally, the conclusion is outlined in Section VII.

II. General View of MMC-Based MTDC Grid

Fig. 1 exhibits an MMC-based four-terminal DC grid. Current limiting inductors (L_{AB}) are located at both ends of each OHL (*A* and *B* are the grid's nodes). In addition, DC Circuit Breakers (DCCBs) are employed to isolate the faulty OHL. The power specifications of the MMC stations and OHL parameters are given in Table I. S_3 is in the DC voltage control mode, and others are in the active power control mode.

The three-phase MMC used to link the AC source to the MTDC grid consists of half-bridge Sub-Modules (SMs). In addition, each MMC phase has two arms, and the arm inductors (L_{arm}) are employed to limit the circulating current [25-26].

III. Fault Detection Strategy

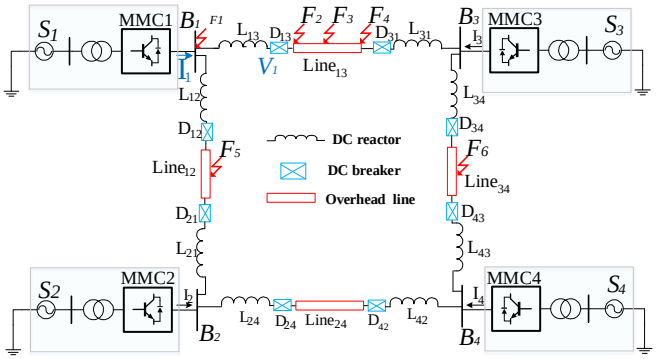

Fig. 1. Configuration of four-terminal MMC-HVDC.

A. ANN Design

ANN is a highly flexible tool designed to solve complicated problems and identify patterns using weights, biases, and activation functions. It is formed of three layers: input, hidden, and output. Each layer has computational processing segments that are named neurons. The input and hidden layer neurons quantity is selected according to the fitting accuracy and error histogram curve, and the output layer neurons quantity is designed according to the entire outputs [25]. The ANN input vector is classified into training, testing, and validation.

As shown in Fig. 2, $R_{j,l}$ is the output of the J^{th} neuron in the l^{th} layer that can be defined as (1). $\omega_{ij,l}$ is the connection weight between the i^{th} and j^{th} neurons in the l^{th} layer, and $b_{j,l}$ is the added bias of j^{th} neurons in the l^{th} layer.

$$R_{j,l} = y\left(\sum_{i=1}^{J_{l-1}} R_{i,l-1}\,\omega_{iJ,l} + b_{J,l}\right) \quad (1)$$

Weights and biases are changed continuously to minimize the pre-defined Minimum Squared Error (MSE) cost function [25]. Towards using Back Propagation (BP) algorithm to train the ANN, the non-linear activation function (tan sigmoid) can be applied according to (2).

$$y(x) = \frac{1}{1 - e^{-x}} \quad (2)$$

In this paper, ANN is utilized for two purposes. The first is for primary fault detection, which is trained according to the different faulty states. Additionally, the second ANN is designed to determine an appropriate threshold according to MTDC grid conditions.

TABLE I
MMC Power Specifications and OHL Lengths

Parameters		Values
DC OHL	Length of OHL13	120km
	Length of OHL12	120km
	Length of OHL24	120km
	Length of OHL34	120km
Active power	Power of S_1	200MW
	Power of S_2	200MW
	Power of S_3	150MW
	Power of S_4	100MW

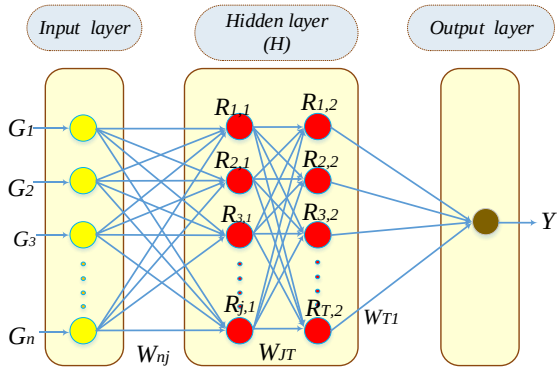

Fig. 2. Three layers perceptron ANN graph.

B. DWT Theory

Wavelet transform has been noticeably utilized in the DC fault detection field due to its ability to evaluate the signal in the time and frequency domains and swift local changes in the faulty signal [6]. Continuous Wavelet Transform (*CWT*) of a signal *f(t)* can be figured.

$$CWT(\lambda,\delta) = \int_{-\infty}^{\infty} f(t) \times \psi^{*}(t)\, dt \tag{3}$$

$$\psi^{*}(t) = |\lambda|{-}1/2 \times \psi\ (\frac{t-\delta}{\lambda})dt \tag{4}$$

Where (λ) and (δ) are scale, and translation parameters, respectively. $\dot{\psi}(t)$ is a daughter wavelet which is the renovated arrangement of the mother wavelet $\psi(t)$ [6].

Based on (3) and (4), the DWT of a discrete signal *f(h)* can be represented as below.

$$DWT(v,k) = (a_0)^{-v/2}(\sum_{h} f[h]\psi[a_0{}^{-v}k - b_0 h]) \tag{5}$$

Where a_0 and b_0 can be assigned *two* and *one*, respectively, and j is the decomposition level. When the Multi-resolution decomposition technique is applied to the discrete signal *f(h)*, the high-frequency detail coefficients can be extracted by the following equation.

$$D_v[h] = \sum_{k=0}^{L-1} A_{v-1}[k] V_v[h-k] \tag{6}$$

Where A_v is the approximation coefficient at level *v*, *L* is the high pass filter order, *V* is the high pass filter, and *h* is the input signal sample. Then the energy of the high-frequency component of the input signal can be written as follows:

$$E_h = \int_{0}^{Tw=1-2ms} D_v[h]^2 dt \tag{7}$$

Among the different mother wavelets, Daubechies2 has been selected due to higher similarity to the faulty signal and less computational burden.

C. DC Reactor Boundary Effect

The DC reactors affect the MTDC grid frequency characteristics. Fig. 3 depicts the MTDC grid simplified equivalent circuit at the internal Pole-to-Pole (PTP) fault instant. It is worth revealing that the superposition theorem is employed for DC fault analysis [10].

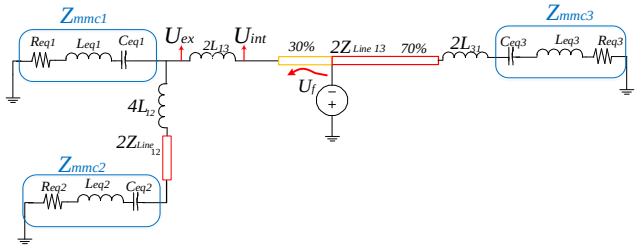

Fig. 3. Simplified model of the MTDC grid during internal DC PTP fault.

Based on the model mentioned earlier, the transfer function between faulty voltage (U_f), the OHL13 inside voltage (U_{int}), and B_1 voltage (U_{ex}) are derived as (8) and (9), respectively.

$$H_{int}(S) = \frac{U_{int}}{U_f} = \frac{Z_{MMC1} \| Z_1 + 2SL_{AB}}{Z_{MMC1} \| Z_1 + 2SL_{AB} + 0.3 \times Z_{line}} \tag{8}$$

$$H_{ex}(S) = \frac{U_{ex}}{U_f} = \frac{Z_{MMC1} \| Z_1}{Z_{MMC1} \| Z_1 + 2SL_{AB} + 0.3 \times Z_{line}} \tag{9}$$

Where Z_{mmcA} (*A*=1, 2, 3, 4) is expressed as (10).

$$Z_{MMC_A} = \frac{1}{3}\left(2SL_{armA} + 2R_{armA} + \frac{N}{2SC_{SMA}}\right) \tag{10}$$

L_{armA}, $R_{armA,}$ *and* C_{SMA} in (8) are arm inductance, resistance, and SM capacitance, respectively. *N* is the SM number per arm. Z_1 also can be defined as follows:

$$Z_1 = Z_{MMC2} + 4SL_{AB} + 2Z_{Line} \tag{11}$$

Based on the described equations, the transfer function ratio between U_{int} and U_{ex} is expressed below:

$$H_{com}(S) = \frac{U_{int}}{U_{ex}} = \frac{Z_{MMC1} \| Z_1 + 2SL_{AB}}{Z_{MMC1} \| Z_1} \tag{12}$$

The bode diagram of the stated transfer functions is illustrated in Fig. 4. As realized, the magnitude frequency characteristic of $H_{ex}(s)$ is similar to the low pass filter, while $H_{int}(s)$ passes all the frequencies. Besides, the $H_{com}(s)$ shows that U_{int} has more high-frequency components than U_{ex} under the internal PTP fault. Consequently, the DC reactor's inherent boundary effectively distinguishes external and internal DC faults.

The proposed fault detection algorithm is designed based on ANN, DWT, and the inherent boundary effect. The strategy procedure is explained in the next section.

IV. Proposed Fault Detection Algorithm

A two-stage fault detection structure is proposed in this article. Different parts of the proposed algorithm (Fig. 5) will be explained in this section.

A. First Stage: Primary Fault Detection

In this subsection, the ANN designing procedure is illustrated as follows:

1-Input Data: The ANN input matrix is extracted by the simulations on the MTDC grid as:

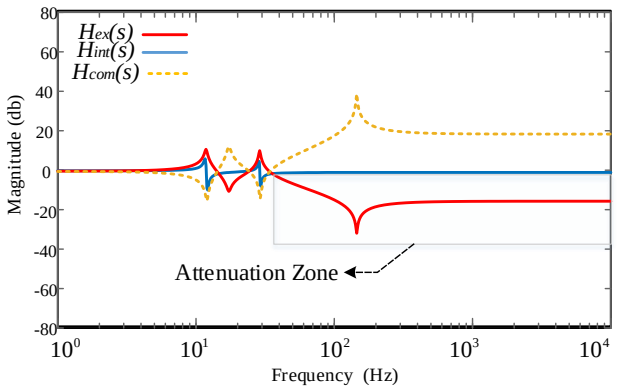

Fig. 4. Frequency analysis of the U_{int}, U_{ex} when the fault occurs.

$$G_{n\times k}=\begin{bmatrix} G_{1,1} & G_{1,2} & G_{1,3} & . & . & . & G_{1,k} \\ G_{2,1} & G_{2,2} & . & . & . & . & . \\ G_{3,1} & . & . & . & . & . & . \\ . & . & . & . & . & . & . \\ . & . & . & . & . & . & . \\ . & . & . & . & . & . & . \\ G_{n,1} & . & . & . & . & . & G_{n,k} \end{bmatrix} \quad (13)$$

$G_{n\times k}$ is the case study matrix with n=3120 rows and k=20 columns representing the number of case studies and the number of voltage samples collected in each simulation. The case study matrix is normalized by (14):

$$\bar{G}_{n\times k}=\frac{G_{n\times k}}{V_{DC}} \quad (14)$$

Where V_{DC} is the nominal DC grid voltage, in addition, a target vector with n rows is defined as:

$$T_{n\times 1}=[T_1,\ldots\ldots,T_n \quad]^T \quad (15)$$

2-Network Training: Each row of the target vector is allotted to an extracted pattern from simulations. The name of the hidden layer is also considered H, and the number of neurons is chosen to be eight based on trials and errors to reach a reasonable accuracy and desired MSE, avoid over-fitting problems, and small delay time. The five pre-fault samples and fifteen post-fault samples are extracted in each simulation. The $R_{j,H}$ is the output value of each neuron in the H layer, which is calculated by the following equation:

$$R_{j,H} \quad =y\left(\sum_{i=1}^{n}\bar{G}_{i(1\times k)}\times\omega_{i\,j(k\times 1)}+b_{j,H}\right) \quad (16)$$

Where J is the number of neurons, $\bar{G}_{i(1\times k)}$ is i^{th} simulation matrix with k columns, and $\omega_{ij(k\times 1)}$ is the weighting matrix. Finally, the output is defined as (17).

Where Z =1 is the number of neurons in the output layer. Considering the output is a function of the equations and formulas of the H layer, the output is defined as $Y=f(H)$.

$$Y=\frac{1}{1-e^{-\left(\sum_{j=1}^{8}R_{J,H}\times\omega_{J,z}\ +b_{z,Y}\right)}}=f(H) \quad (17)$$

The ANN's output is expressed through a linear activation function according to (18). The fault with the highest severity is assigned to the lowest target value (0.6), and the faulty event with the lowest severity is allocated to the target value (0.95).

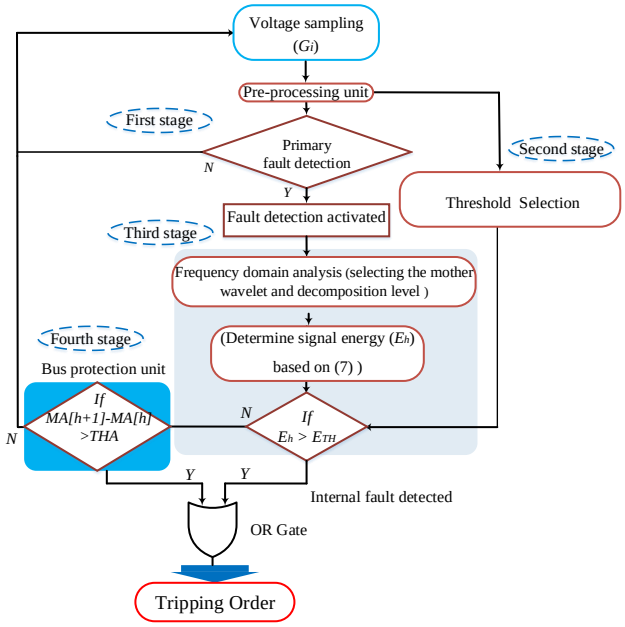

Fig. 5. Overall view of the proposed fault detection algorithm.

The target value for the non-faulty states is also considered between (0.1) and (0.35).

$$Y=f(H)=\begin{cases}0.1<Y<0.35 & \text{Non-faulty state}\\ 0.6<Y<0.9 & \text{faulty state}\end{cases} \quad (18)$$

3-Training Results: The Levenberg-Marquardt training algorithm is employed to optimize weights and biases. Fig. 6 demonstrates the simulation results of the designed network for incipient fault detection. The training performance is illustrated in Fig. 6(a). MSE is determined at each learning period and stopped when it reaches its minimum value. Furthermore, the correlation coefficient curve of the designed ANN is depicted in Fig. 6(b). The regression index =0.9986 is obtained in the desired range.

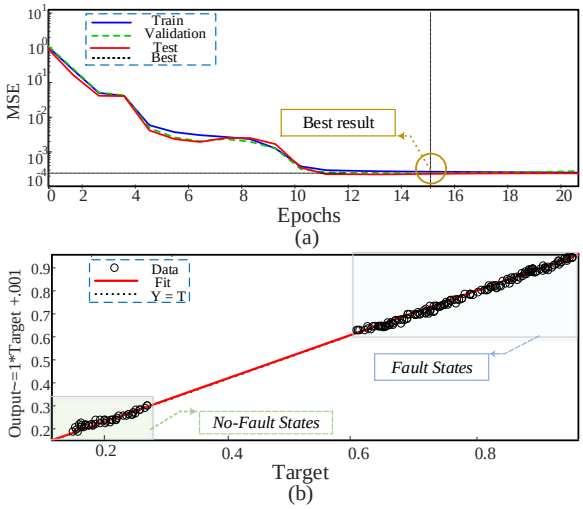

Fig. 6. Training results for the primary detection: (a) MSE curve, (b) Correlation curve of the trained network.

TABLE II
SOME OF THE PRIMARY FAULT DETECTION CASE STUDIES

Each X=2% of OHL13 with R_f=5Ω, 25Ω, 50Ω, 75Ω and 100Ω	Fault at X% OHL13 with fault resistance R_f	Faulty states
Each R_f=0.5Ω of 5< R_f <100 at X=5%, 10%, 50%, 75% and 100%		
Increase and decrease the active power of MMC_1, MMC_2, MMC_3, and MMC_4 by 5% to 50%	Abrupt active power change of MMCs	Non-faulty states
Increase and decrease load power consumption by 5% to 50%	Flexible load variation	
Abrupt input and exit of MMC_1, MMC_2, MMC_3, MMC_4	Input and output of each MMCs	
Exit of the OHL12, OHL13, OHL34, and OHL24	The exit of adjacent OHL	

After the input samples are normalized in the pre-processing unit, they are used in the first ANN. The input patterns to the ANN are updated at each sampling frequency.S

B. Second Stage: Threshold Selection

The fixed value threshold used in the existing methods is unreliable in different grid conditions. From Fig. 7(a), 210 is the chosen value for threshold (E_{TH}) in normal conditions. This value is a suitable criterion for discriminating internal and external faults within the protection zone of OHL13. The considerable difference between E_{TH} and E_{int} satisfies the condition required for the final decision. Figs. 7(b) to (d) show that when MMC_1, MMC_2, and MMC_3 exit the DC grid, the fault energy varies highly in all fault locations, mainly when a fault is applied in 20%, 80% of OHL13, and at B_3. In Figs. 7(e) and (f), the load power tied at the beginning of OHL13 is increased by 25% and 50%, respectively. As shown in both cases, in some parts of OHL13, the minimum amount of fault energy compared with the fixed value threshold is less than this value. Thus, it is not recognized as an internal fault within the protection zone of OHL13. As a result, it causes malfunction.

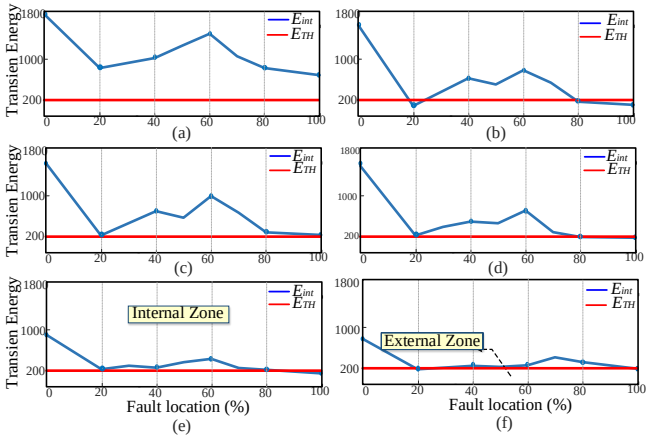

Fig. 7. Internal fault energy at different locations of OHL13 (with R_f=100Ω): (a) Normal state, (b) MMC_1 exit, (c) MMC_2 exit, (d) MMC_3 exit, (e) 25% load increase, (f) 50% load increase.

The ANN method is proposed to solve the mentioned problem, which determines the threshold value in different grid conditions. By finding the corresponding pattern between variations of the MTDC grid parameters and their influence on the grid voltage by the second ANN, the threshold value is updated. To do this, a particular target value is assigned to each pattern of input data by writing code in the MATLAB/Script environment. First, the input samples are sorted according to the severity of the fault. Then the values between 0.6 and 0.9 are assigned to them in a separate vector named the target vector. The same procedure has been done for the non-faulty state.

The designed ANN has two hidden layers with six neurons in each layer. Also, the MSE =0.9952 is the best training performance at epoch 36. Moreover, the second ANN specification is provided in Table III.

When the MTDC grid condition changes, the related voltage pattern is analyzed by the second ANN, and the corresponding thresholSd value is determined. Then, the updated threshold value is sent to the DWT section.

Considering 1ms for the fault detection data window, the minimum updating rate for the threshold value can be chosen as 1ms to make an effective performance for the threshold selection unit.

TABLE III
SPECIFICATIONS OF THE SECOND ANN

No. of inputs	11500
No. of hidden layer	2
No. of neurons	6
Activation function	Tan sigmoid
Learning algorithm	Levenberg-Marquardt
Cost function	MSE

C. Third Stage: DWT Section

As previously clarified, the DC inductor boundary effect is an excellent approach to discriminating between internal and external faults. The signal energy is figured according to equation (7) and compared to a threshold value. The appropriate criterion is the most severe fault that occurred beyond the protection zone (PTP metallic fault energy with R_f= 0Ω at B_1 (=E_{hmin})), and the high resistance fault happened inside the OHL13 (with R_f=100Ω (=E_{int})). These values are compared, and the internal or external fault detection is determined. Notably, the reliability coefficient (K_r=2.5) for disorders and noise coverage are also considered for the final threshold value calculation.

$$E_{TH}=K_r \times E_{hmin} \quad (19)$$

TABLE IV
TRAINED THRESHOLD VALUES

Grid state	Target	Output	Relative error (%)
MMC_1 exit	96	97.25	1.2
MMC_2 exit	101	102.3	1.46
MMC_3 exit	115	114.2	0.7
OHL12 exit	150	152.3	1.31
Load power increase (25%)	52	51.1	1.17
Load power increase (50%)	35	34.6	1.1
MMC_1 power increase (25%)	141	140.5	0.3
Normal state	210	208.9	0.5

Finally, this value is compared to the second ANN's determined threshold value. The results show whether the internal fault occurs or not. Some of the trained threshold values are listed in Table IV. It provides training results on the grid's normal and abnormal states. It should be noted that the target value is chosen based on the metallic external fault energy that is known as the most severe PTP DC fault. The maximum relative error between targets and output values is 1.46%, indicating that the training is well done. As a result, the threshold values will be compatible with different MTDC grid conditions. Other scenarios influence the threshold value, such as changing the OHL13 parameters and the DC inductor. However, they occur less frequently in the grid and are not in the scope of this paper.

D. Fourth Stage: Bus Protection Unit

Due to the low impedance, the bus fault is regarded as the most severe fault in the MTDC grid. During this interval, all DCCBs connected to the faulty bus must operate to separate the defective segment from the other grid parts to prevent the DC grid from collapsing. According to the flowchart in Fig. 5, the bus protection unit is triggered when a non-internal fault is detected. In this case, the sum of the bus currents is checked according to (20) and (21).

$$M_A[h] = \sum I_{AB}[h] + I_B[h] \tag{20}$$

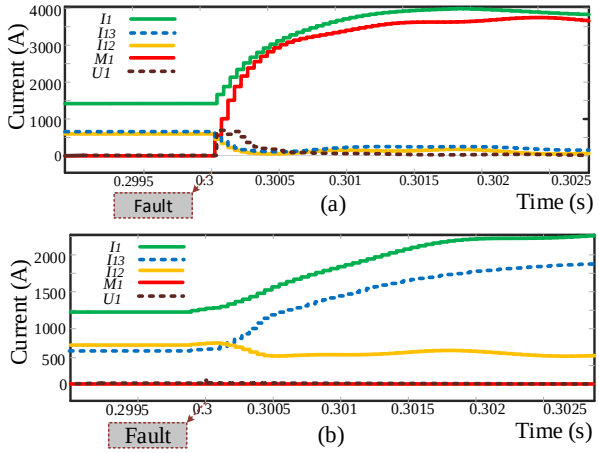

Fig. 8. Current measurement during various faults: (a) PTP DC bus fault, (b) PTP DC OHL fault.

$$U_A = |M_A[h+1] - M_A[h]| > TH_A \tag{21}$$

Where I_{AB} is the OHL current and I_B is the converter current. TH_A is considered a bit more than zero to nullify the noise influence. If U_A is close to zero, it indicates that a fault has happened in the adjacent OHL, and if it is considerably higher than zero, the bus fault has occurred, and the command is sent to the DCCBs connected to the faulty bus. Fig. 8(a) and (b) describe the converter current (I_1), OHL13 current (I_{13}), OHL12 current (I_{12}), and the bus current (M1) at B1 and 50% of OHL13, respectively. As seen, when a fault occurs at the DC bus, the bus current rises significantly (red line in Fig. 8(a)), and when a DC fault is applied at the OHL13, the bus current is nearby to zero (red line in Fig. 8(b)). Therefore, it is a suitable criterion for distinguishing the bus and OHL faults. Since the corresponding DCCB takes commands from two ways (internal fault or bus fault), a logical gate (OR) is utilized in the proposed algorithm.

Counter Function: It is an independent setting value used in each ANN unit to prevent ANN's incorrect decision caused by the ANN's training errors, noise, and other transient effects in the MTDC grid. In other words, the counter function is employed to guarantee the reliable performance of the primary fault detection. The threshold value for the counter function is selected as 0.5. The counter function classifies the ANN's output higher than 0.5 as a faulty state and lower than 0.5 as a non-faulty state.

V. SIMULATION RESULTS AND PERFORMANCE EVALUATIONS

A four-terminal MMC-based MTDC grid is used to verify the proposed algorithm's effectiveness. The prototype system is simulated in MATLAB/ SIMULINK environment. The MTDC grid parameters are listed in Table V.

A. Primary Fault Detection Evaluation

In the first stage, the primary fault detection capability of the proposed algorithm is elaborated. Fig. 10 shows both voltage and ANN output behaviors in different scenarios. Fig. 9(a) shows a 10Ω PTP fault applied at 20% of OHL13 at t=0.3s. The voltage V_1 has suddenly dropped to below 0.6(p.u.). Meanwhile, the ANN output has reached the value of 0.58. Although this value is out of the equation (18) range caused by ANN's training error, this event is known as a fault using the counter value (=0.5). Also, the detection delay is 0.3ms, which is reasonable for primary detection. As it is indicated in Figs. 9(b), when the 90Ω DC PTP fault is applied at the previous location, the corresponding ANN's output exceeds the counter value. Thus, the proposed method successfully detects the DC PTP fault with a broad range of fault resistances. Consequently, the robustness of the proposed approach is satisfied. Fig. 9(c) reveals the active power change of MMC_1 and MMC_3 by 20%. Fig. 9(d) also exemplifies the sudden exit of the MMC_2. Evidence indicates that ANN's outputs are well below the counter value. Therefore, they cannot trigger the fault detection algorithm. Figs. 9(e) and (f) demonstrate how flexible load changes affect the ANN's output. The ANN's outputs for 15 and 50 percent load increase are 0.28 and 0.33, respectively, below the counter value. Therefore, the ANN design for primary fault

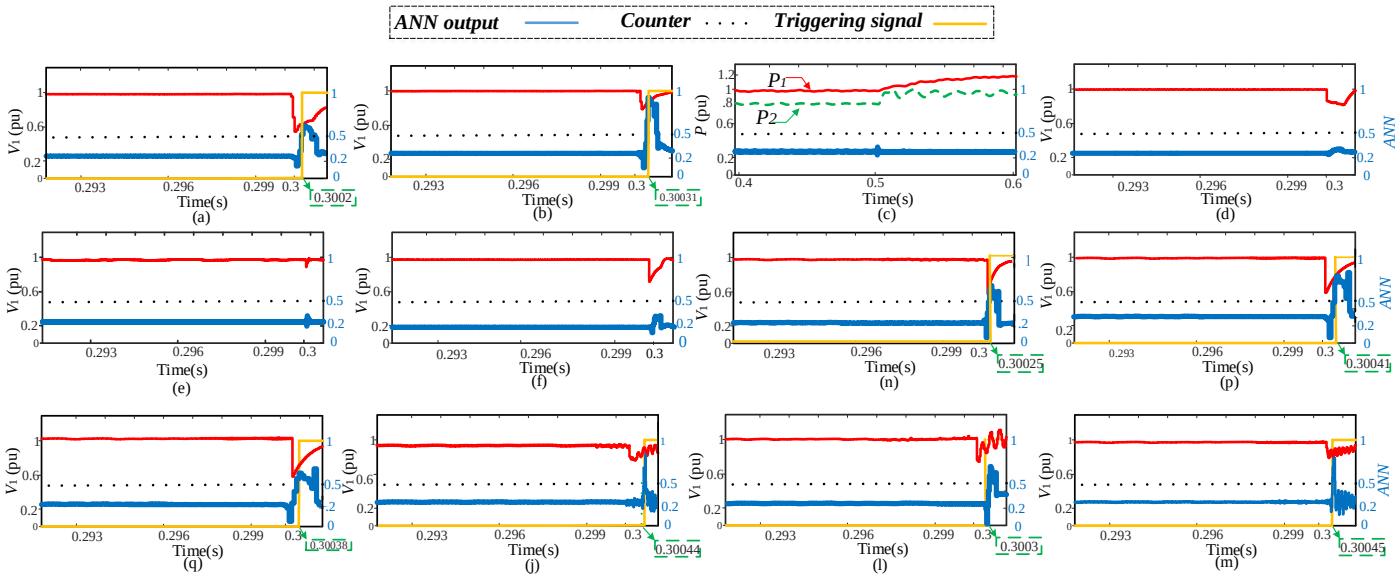

Fig. 9. Simulation for the primary detection: (a) PTP fault with R_f=10Ω, (b) PTP fault with R_f=90Ω, (c) MMC_1 and MMC_3 active power change, (d) MMC_2 abrupt exit, (e) 15% of load increase, (f) 50% of load increase, (n) PTP fault (R_f=0.5 Ω) when the load increases 50% (p) PTP fault (R_f=0.5 Ω) when the MMC_2 exits, (q) PTP fault (R_f=0.5 Ω) when the OHL34 exits, (j) P-PTG fault (R_f=0.5 Ω) when the load increases 50%, (l) P-PTG fault (R_f=0.5 Ω) when the OHL34 exits, (m) N-PTG fault (R_f=0.5 Ω) when the OHL34 exits.

detection is done correctly, proving the high reliability against the non-faulty states.

Different DC faults have been applied to the grid's abnormal conditions to study the proposed method's performance. For instance, Figs. 9(n) to (q) show the accurate performance of the primary fault detection when the PTP DC fault is applied in abnormal conditions. In addition, Positive-Pole-to-Ground (P-PTG) and Negative-Pole-to-Ground (N-PTG) faults are also applied on OHL13 and illustrated in Figs. 9(j) to (m), indicating the successful operation of the proposed method to recognize the other types of faults in abnormal grid conditions.

B. Robustness Evaluation

This section investigates the proposed method's robustness against the vast range of fault resistances. To make a fair assessment, first, the fault resistances are per-united by the following equation:

$$Z_{base} = \frac{V^2_{rated}}{P_{rated}} \quad (22)$$

P_{rated} and V_{rated} are the grid's nominal active power and voltage. 4.59p.u. is the corresponding per-united value to 100Ω fault resistance, and the 50p.u. is related to 1089Ω fault resistance. Fig. 10(a) shows the robustness of the proposed method against the P-PTG, N-PTG, and PTP DC faults.

The proposed fault detection accuracy rate is guaranteed up to R_f=4.59 p.u. As the fault resistance increases, the accuracy rate diminishes. The minimum accuracy rate corresponds to the PTG faults, which is 81.5%. Because it is a high-resistance fault, it cannot seriously damage the MTDC grid. Therefore, the DWT scheme can recognize it in the next stage of the proposed algorithm.

C. Impact of Sampling Frequency

As mentioned in section IV, the sampling frequency employed in this research is 20 kHz. As shown in Figs. 10(b), when the number of input samples decreases (from 15 to 5), the accuracy rate of the proposed method reduces. The minimum accuracy rate is 84.7% when the PTP DC fault with R_f= 80Ω is applied at 60% of OHL13. Although the accuracy rate is decreased, the DWT section is considered in the proposed fault detection algorithm to compensate for the possible errors that occurred by insufficient input samples. In other words, protection performance is also reliable when the input samples decrease by 75%.

D. Influence of Noise

Practical measurements are usually done in the presence of noise. The Gaussian white noise is added to the measured signals to verify the proposed method's immunity against the noise. The Signal-to-Noise Ratio (*SNR*) is employed to describe the noise level in a measured signal. The simulations with *SNR*=15dB are performed, and the results are provided in Table VI. As comprehended, threshold values are different in diverse MTDC grid conditions. Since the designed algorithm is adjustable to changes in grid parameters, reducing the possibility of mal-

TABLE V
MTDC SYSTEM PARAMETERS

Symbol	System Parameter	Value
P_g	Rated active power	200 MW
V_{DC}	Rated DC voltage	±200 kV
V_{LL}	Rated AC voltage	66 kV
N	Number of SMs in each arm	100
L_{arm}	Arm reactor	5 mH
C_{SM}	SM Capacitor	12 mF
L_{line}	Line inductor	.8 mH/Km
R_{line}	Line resistor	15 mΩ/Km
L_{AB}	Current limiting inductor	40 mH
f_s	Sampling frequency	20 kHz
f	AC voltage frequency	50Hz

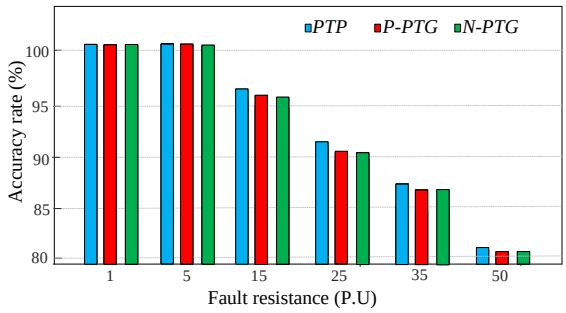

(a)

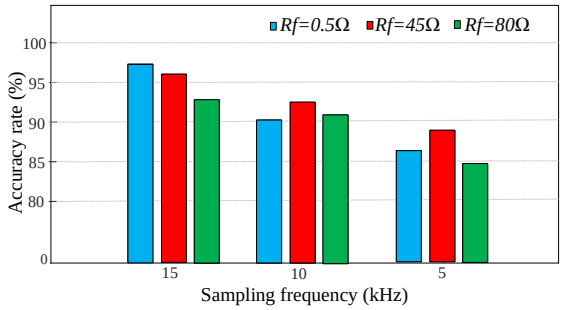

(b)

Fig. 10. Performance evaluation of the proposed method at (a) The vast range of fault resistance, (b) Different sampling frequencies.

operations in the protection system. Besides, as seen in Table VI, the proposed algorithm accurately identifies the fault type (internal or external) at different fault resistances and locations that guarantee the selectivity of the proposed algorithm. Moreover, the bus protection unit's performance is provided in the last column of Table VII. As demonstrated, it correctly recognizesthe external fault type (bus fault or adjacent OHLfault), preventing complete grid failure during the severe PTP bus fault.

Also, the primary fault detection's accuracy against the variations of the SM capacitor size (from 22mF to 5mF) is investigated. The results indicate that the proposed method is accurate and robust against the vast range of the SM capacitor size.

As previously stated, two simple ANNs structures (in terms of the number of neurons and hidden layers) and local data are employed for fault detection. Hence, it is desired that the fault detection delay be small. Table VII shows that the detection delay range is 1.21~2.29ms, which is reasonable for fault recognition.

VI. Performance Comparison and Discussion

In this section, the proposed method is compared with existing ANN, DWT-ANN, and non-ANN-based fault detection approaches to verify its advantages. To make a fair comparison, the competitors' parameters are per-united according to the corresponding nominal voltage and active power. It is due to differences in the parameters of the case studies.

A. Comparison with ANN and ANN-DWT-Based Methods

In [25-27], a fixed value threshold is chosen for the primary fault detection based on voltage derivative, which is unreliable against intense noises, system transients, and high resistance faults. However, in the proposed scheme, an ANN method with a comprehensive case study including the non-faulty states is employed for primary fault detection. In addition, [25] and [26] used a fixed value threshold for confirmation commands vulnerable to the system parameter variation. As said, it affects the reliability of the protection system. However, this paper employs a straightforward, simple, and reliable method based on ANN to solve the fixed value threshold problems. On the other hand, except for [27] and the proposed method, all other methods do not have a bus protection unit, which is critical in the protection system, as the bus fault is the most severe DC fault.

Four ANN and ANN-DWT-based fault detection methods are implemented in a similar case study. Afterward, the MTDC grid parameter variations are analyzed. As it is shown in Fig. 11, the accuracy rate of the proposed method is higher

TABLE VII
Performance of the Proposed Algorithm During a DC PTP Fault (D13)

Noise (SNR)	Grid state		Fault location	Fault resistance (Ω)	Transient energy (kV^2)	Determined threshold	Fault type Correct (✓)	Bus protection unit	Detection delay (ms)
15 dB	Normal		*F1*	0	117.5	208.9	External (✓)	Bus fault	1.21
			F4	100	689	208.9	Internal (✓)	Not activated	2.18
			F6	43	87	208.9	External (✓)	Adjacent OHL fault	2.29
			F2	32	2750	208.9	Internal (✓)	Not activated	1.65
			F3	55	2023	208.9	Internal (✓)	Not activated	1.86
			F5	18	121	208.9	External (✓)	Adjacent OHL fault	2.01
	Abnormal	Load increase (50%)	*F4*	64	331	34.6	Internal (✓)	Adjacent OHL fault	2.25
			F3	20	402	34.6	Internal (✓)	Not activated	1.89
		MMC_1 exit	*F1*	20	99.1	96	External (✓)	Not activated	1.45
			F2	0	2202	96	Internal (✓)	Bus fault	1.61
		OHL34 exit	*F2*	80	1741	174	Internal (✓)	Not activated	1.68
			F1	12	169.2	174	External (✓)	Not activated	1.45
		MMC_1 power change (25%)	*F6*	50	78.3	140.5	External (✓)	Bus fault	2.29
			F5	30	89	140.5	External (✓)	Adjacent OHL fault	2.05

than 98.7 % while the accuracy of other methods is lower than 91% for the same condition. Also, 81.4% is the minimum accuracy rate corresponding to [23]. The results confirm that the proposed method is more accurate than the other fault detection algorithms.

In addition, the noise effect is not investigated in [23], [24], and [26], while the proposed method's performance is verified in the presence of white Gaussian noise when the SNR=15 dB. Besides, the robustness of the proposed method against the fault resistance is verified up to 4.59p.u. The results show a nearly 100% accuracy rate. Authors in [27] reported an accuracy rate of 84.5% at fault with 6p.u resistance, while the proposed method has a 96.4% accuracy at this fault resistance, confirming the superior robustness of the proposed approach. Authors in [28] presented a fault detection approach robust to noise disturbance and high resistance fault. However, its average fault detection time (= 2.047ms) is higher than the proposed method (= 1.81ms). The summary of comparisons is provided in Table VIII.

A. Comparison with Non-ANN-Based Methods

The local data-based protection algorithm is proposed in this paper, while in [10], the high sampling rate communications links are needed, which causes more implementation complexity and cost. In addition, [10] used a high sampling frequency (500 kHz), increasing system implementation expenses and complexities. Moreover, it uses fixed value thresholds. In [18] and [4], the fixed value threshold is adjusted for the confirmation command

of each relay. In addition, a fixed value threshold is used as an activating criterion for triggering the fault detection algorithm. Noises or other transients may affect this criterion. However, the proposed method is accurate and robust against fault resistances and noise levels and solves the fixed value threshold problems, increasing the protection system's reliability.

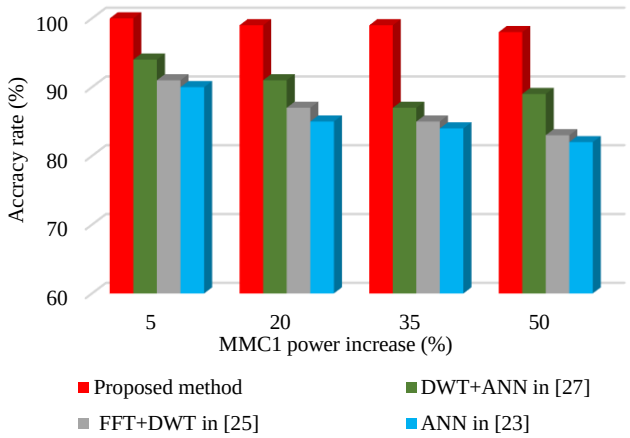

Fig. 11. Comparison between the accuracy rate of four methods in terms of grid parameters variation.

VII. Conclusion

This article proposes a novel fault detection algorithm for an MMC-based MTDC grid. The critical contributions of the proposed algorithm are enumerated below:

TABLE VIII
Comparison with ANN and ANN-DWT-Based Fault Detection Methods

DC fault detection method	Algorithm activating (robustness to non-faulty cases)	Threshold selection (grid condition changes enduring)	Bus protection	Fault resistance robustness – capability (p.u.)	Noise endurance (SNR)	Considerations
ANN in [23]	Direct faulty samples (Low)		╳	Low (Up to 0.17)	Not verified	• Multiple ANNs are used (13 units). • High workload. • Direct use of faulty samples for fault detection.
ANN in [24]	Direct faulty samples (Low)		╳	Low (Up to 0.68)	Not verified	• A low number of case studies was selected. • The noise effect is not studied.
FFT+ANN in [25]	fixed value threshold (Low)	Fixed FFT energy value-based (Low)	╳	Low (Up to 2.06)	Low (50dB)	• High fault detection delay (about 4ms). • Non-comprehensive case studies.
DWT + Fuzzy-Neural in [26]	fixed value threshold (Low)	Fixed DWT energy value-based (Low)	╳	Low (Up to .04)	Not verified	• High sampling frequency rate (50 kHz). • Complex fault detection algorithm. • Low operability.
DWT + ANN in [27]	fixed value threshold (Low)	ANN based (High)	√	High (Up to 4.2)	High (18dB)	• Low recognition rate at high resistance fault (84.5% at 6 p.u.). • Grid parameter variations are not considered.
Proposed ANN + DWT method	ANN based (High)	ANN based (High)	√	High (Up to 4.59)	High (15dB)	• Robust against a vast range of fault resistances. • allowable fault detection delay (1.21-2.29ms).

- The ANN method will increase the MTDC grid protection reliability by eliminating the fixed value thresholds.
- The highly robust protection scheme is provided by training numerous faulty states and other abrupt changes in MTDC grid parameters named non-faulty states.
- The bus protection unit discriminates between the bus fault and the adjacent OHL fault.
- A high-speed communication link is not required using the local measurement, which decreases the implementation cost and omits communication delays.
- The fault detection delay is small as a fault detection scheme is employed using two simple ANNs and local data.

DWT also extracts the transient signal's high-frequency components to calculate the fault energy. Numerous simulations have been conducted, and the results confirm the proposed method's achievements validating the suggested algorithm performance.

VII. Reference

[1] M. Langwasser, G. De Carne, M. Liserre, and M. Biskoping, "Fault Current Estimation in Multi-Terminal HVdc Grids Considering MMC Control," *IEEE Trans. Power Syst.*, vol. 34, no. 3, pp. 2179–2189, May 2019.

[2] C. Zhang, J. Huang, G. Song, and X. Dong, "Non-Unit Ultra-High-Speed Line Protection for Multi-Terminal Hybrid LCC/MMC HVDC System and Its Application Research," *IEEE Trans. Power Deliv.*, vol. 36, no. 5, pp. 2825–2838, Oct. 2021.

[3] G. P. Adam, T. K. Vrana, R. Li, P. Li, G. Burt, and S. Finney, "Review of technologies for DC grids – power conversion, flow control and protection," *IET Power Electron.*, vol. 12, no. 8, pp. 1851–1867, Jul. 2019.

[4] S. Yang, W. Xiang, and J. Wen, "An Improved DC Fault Protection Scheme Independent of Boundary Components for MMC Based HVDC Grids," *IEEE Trans. Power Deliv.*, vol. 36, no. 4, pp. 2520–2531, 2021.

[5] W. Xiang, S. Yang, G. P. Adam, H. Zhang, W. Zuo, and J. Wen, "DC Fault Protection Algorithms of MMC-HVDC Grids: Fault Analysis, Methodologies, Experimental Validations, and Future Trends," *IEEE Trans. Power Electron.*, vol. 36, no. 10, pp. 11245–11264, Oct. 2021.

[6] B. Li, Y. Li, J. He, and W. Wen, "A Novel Single-Ended Transient-Voltage-Based Protection Strategy for Flexible DC Grid," *IEEE Trans. Power Deliv.*, vol. 34, no. 5, pp. 1925–1937, Oct. 2019.

[7] D. Marques da Silva, F. B. Costa, V. Miranda, and H. Leite, "Wavelet-based analysis and detection of traveling waves due to DC faults in LCC HVDC systems," *Int. J. Electr. Power Energy Syst.*, vol. 104, pp. 291–300, Jan. 2019.

[8] Y. Zhang, Y. Li, J. Song, B. Li, and X. Chen, "A New Protection Scheme for HVDC Transmission Lines Based on the Specific Frequency Current of DC Filter," *IEEE Trans. Power Deliv.*, vol. 34, no. 2, pp. 420–429, 2019.

[9] M. Mehrabi-Kooshki, S. S. Mirhosseini, and S. Jamali, "Non-unit protection scheme for HVDC transmission lines based on energy of voltage difference," *IET Gener. Transm. Distrib.*, vol. 16, no. 11, pp. 2166–2187, 2022.

[10] X. Pei, H. Pang, Y. Li, L. Chen, X. Ding, and G. Tang, "A Novel Ultra-High-Speed Traveling-Wave Protection Principle for VSC-based DC Grids," *IEEE Access*, vol. 7, pp. 119765–119773, 2019.

[11] W. Xiang, S. Yang, L. Xu, J. Zhang, W. Lin, and J. Wen, "A Transient Voltage-Based DC Fault Line Protection Scheme for MMC-Based DC Grid Embedding DC Breakers," *IEEE Trans. Power Deliv.*, vol. 34, no. 1, pp. 334–345, Feb. 2019.

[12] M. J. Perez-Molina, D. M. Larruskain, P. Eguia, and V. Valverde Santiago, "Local Derivative-Based Fault Detection for HVDC Grids," *IEEE Trans. Ind. Appl.*, vol. 58, no. 2, pp. 1521–1530, 2022.

[13] Q. Huang, G. Zou, X. Wei, C. Sun, and H. Gao, "A non-unit line protection scheme for MMC-based multi-terminal HVDC grid," *Int. J. Electr. Power Energy Syst.*, vol. 107, no. May 2018, pp. 1–9, May 2019.

[14] N. Tong *et al.*, "Local Measurement-Based Ultra-High-Speed Main Protection for Long Distance VSC-MTDC," *IEEE Trans. Power Deliv.*, vol. 34, no. 1, pp. 353–364, Feb. 2019.

[15] N. M. Haleem and A. D. Rajapakse, "Fault-Type Discrimination in HVDC Transmission Lines Using Rate of Change of Local Currents," *IEEE Trans. Power Deliv.*, vol. 35, no. 1, pp. 117–129, Feb. 2020.

[16] K. Satpathi, Y. M. Yeap, A. Ukil, and N. Geddada, "Short-Time Fourier Transform Based Transient Analysis of VSC Interfaced Point-to-Point DC System," *IEEE Trans. Ind. Electron.*, vol. 65, no. 5, pp. 4080–4091, May 2018.

[17] D. Li, A. Ukil, K. Satpathi, and Y. M. Yeap, "Improved S Transform-Based Fault Detection Method in Voltage Source Converter Interfaced DC System," *IEEE Trans. Ind. Electron.*, vol. 68, no. 6, pp. 5024–5035, Jun. 2021.

[18] V. Psaras, D. Tzelepis, D. Vozikis, G. P. Adam, and G. Burt, "Non-Unit Protection for HVDC Grids: An Analytical Approach for Wavelet Transform-Based Schemes," *IEEE Trans. Power Deliv.*, vol. 36, no. 5, pp. 2634–2645, 2021.

[19] R. Bertho, V. A. Lacerda, R. M. Monaro, J. C. M. Vieira, and D. V. Coury, "Selective Nonunit Protection Technique for Multiterminal VSC-HVDC Grids," *IEEE Trans. Power Deliv.*, vol. 33, no. 5, pp. 2106–2114, Oct. 2018.

[20] W. Xiang, S. Yang, L. Xu, S. Member, J. Zhang, and W. Lin, "A Transient Voltage based DC Fault Line Protection Scheme for MMC based DC Grid Embedding DC Breakers," no. October, 2018.

[21] S. Wang, T. Dragicevic, Y. Gao, and R. Teodorescu, "Neural Network Based Model Predictive Controllers for Modular Multilevel Converters," *IEEE Trans. Energy Convers.*, vol. 36, no. 2, pp. 1562–1571, Jun. 2021.

[22] I. S. Mohamed, S. Rovetta, T. D. Do, T. Dragicević and A. A. Z. Diab, "A Neural-Network-Based Model Predictive Control of Three-Phase Inverter With an Output *LC* Filter," in *IEEE Access*, vol. 7, pp. 124737-124749, 2019.

[23] V. L. Merlin, R. C. Dos Santos, S. Le Blond, and D. V. Coury, "Efficient and robust ANN-based method for an improved protection of VSC-HVDC systems," *IET Renew. Power Gener.*, vol. 12, no. 13, pp. 1555–1562, 2018.

[24] R. C. Santos, S. Le Blond, D. V. Coury, and R. K. Aggarwal, "A novel and comprehensive single terminal ANN based decision support for relaying of VSC based HVDC links," *Electr. Power Syst. Res.*, vol. 141, no. January 2018.

[25] Q. Yang, S. Le Blond, R. Aggarwal, Y. Wang, and J. Li, "New ANN method for multi-terminal HVDC protection relaying," *Electr. Power Syst. Res.*, vol. 148, pp. 192–201, Jul. 2017.

[26] A. Hossam-Eldin, A. Lotfy, M. Elgamal, and M. Ebeed, "Artificial intelligence-based short-circuit fault identifier for MT-HVDC systems," *IET Gener. Transm. Distrib.*, vol. 12, no. 10, pp. 2436–2443, 2018.

[27] W. Xiang, S. Yang, and J. Wen, "ANN-based robust DC fault protection algorithm for MMC high-voltage direct current grids," *IET Renew. Power Gener.*, vol. 14, no. 2, pp. 199–210, Feb. 2020.

[28] J. Li, G. Song, J. Yan, Y. Li and Z. Xu, "Data-Driven Fault Detection and Classification for MTDC Systems by Integrating HCTSA and Softmax Regression," *IEEE Trans. Power Deliv.*, vol. 37, no. 2, pp. 893-904, April 2022.

Alireza Pourfaraj received both B.Sc. and M.Sc. degrees in electrical engineering from Ferdowsi University of Mashhad, Iran, in 2016 and 2018, respectively, in power electronics.

He is currently pursuing the Ph.D. degree in electrical engineering with the School of Electrical and Computer Engineering, University of Tehran, Iran. His research interests include HV-MTDC grid control and protection and power electronics.

Hossein Iman-Eini (M'10-SM'17) received the Ph.D. degree in electrical engineering jointly from the University of Tehran,Tehran, Iran, and the Grenoble Alpes University, Grenoble, France, in 2009. He is currently an Associate Professor of electrical engineering with the School of Electrical and Computer Engineering, University of Tehran. His current research interests include the modelling and control of power converters, renewable energy systems, and applications of power electronics in power systems.

Sattar Bazyar received the B.Sc. and M.Sc. degrees in electrical engineering with honors from the University of Tehran, Tehran, Iran, in 2018 and 2020, respectively. He is currently a Ph.D. candidate and Scientific Staff Member at the Chair of Power Electronics, Christian-Albrechts-Universität of Kiel, Kiel, Germany. His current research interests include multilevel power converters, and HVdc systems.

Saeid Ahmadi received the B.Sc. degree in electrical engineering from Tehran University, Tehran, Iran, in 2018, and the M.Sc. degree in electrical engineering from the University of Tehran, Tehran, Iran, in 2020. He is currently pursuing the Ph.D. degree in electrical engineering at University of Tehran, Tehran, Iran. His current research interests include advanced control for modular multilevel converters.

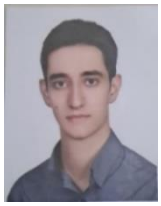

Ehsan Asadi received the B.Sc. degree in electrical engineering from Isfahan University of Technology, Isfahan, Iran, in 2017, and the M.Sc. degree in electrical engineering from the University of Tehran, Tehran, Iran, in 2020. He is currently a Research Assistant at the School of Electrical and Computer Engineering, University of Tehran. His research interests include applications of power electronics in power systems.

Marius Langwasser (S'16, M'22) received the M.Sc. and Ph.D. degrees from Kiel University, Kiel, Germany, in 2016 and 2021, respectively. He is currently a Senior Post-Doctoral Scientific Staff Member and the Leader of the Group "Hybrid Grids," Chair of Power Electronics, Kiel University. He is responsible for the Kopernikus-project ENSURE and Marie Sklodowska-Curie Research Actions Wingrid and SMARTGYsum. His research interests include control and protection of meshed and hybrid grids, and smart transformers.

Marco Liserre (S'00-M'02-SM'07-F´13) received the MSc and PhD degree in Electrical Engineering from the Bari Technical University, respectively in 1998 and 2002. He has been Associate Professor at Bari Technical University and from 2012 Professor in reliable power electronics at Aalborg University (Denmark). From 2013 he is Full Professor and he holds the Chair of Power Electronics at Kiel University (Germany). He got offered and declined professorships at the Technical Universities of Ilmenau, Munich and Hamburg. He has published more than 600 technical papers (1/3 of them in international peer-reviewed journals), a book and 2 granted Patents, with more under evaluation, some of them involving companies. These works have received more than 49000 citations. Marco Liserre is listed in ISI Thomson report "The world's most influential scientific minds" from 2014. In 2022 he joined part-time Fraunhofer ISIT as Deputy Director and Director of a new Center for "Electronic Energy Systems" funded for 5 Million Euro.

He is member of IAS, PELS, PES and IES. He has been serving all these societies in different capacities. In PELS he is AdCom member (second mandate), Co-Editor of the IEEE Open Access Journal in Power Electronics, Associate Editor of TPEL and JESTPE, Guest Editor of Several Special Issues of JESTPE, Technical Committee Chairman of the new Committee on Electronic Power Grid Systems and Member of the IEEE Digital Committee, IES-Liaison responsible, eGrid 2021 Workshop Co-chairman and PEDG 2022 Co-chairman and organizer in Kiel. He has received the IES 2009 Early Career Award, the IES 2011 Anthony J. Hornfeck Service Award, the 2014 Dr. Bimal Bose Energy Systems Award, the 2017 IEEE PELS Sustainable Energy Systems Technical Achievement Award, the 2018 IEEE-IES Mittelmann Achievement Award and 6 IEEE Journal Awards.